

# Carotid Atherosclerotic Plaque Vulnerability Assessment Using 3D Thin-Layer Model with In Vivo Patient-Specific Vessel Material Properties

\*Qingyu Wang,<sup>1</sup> Gador Canton,<sup>2</sup> Thomas S. Hatsukami,<sup>3</sup> Kristen L Billiar,<sup>4</sup>  
Chun Yuan,<sup>5</sup> Zheyang Wu,<sup>6</sup> †Dalin Tang<sup>1,6</sup>

<sup>1</sup> School of Biological Science and Medical Engineering, Southeast University, Nanjing, 201196, China

<sup>2</sup> Department of Mechanical Engineering, University of Washington, Seattle, WA 98195

<sup>3</sup> Division of Vascular Surgery, University of Washington, Seattle, WA. 98195

<sup>4</sup> Biomedical Engineering Department, Worcester Polytechnic Institute, Worcester, MA 01609 USA

<sup>5</sup> Department of Radiology, University of Washington, Seattle, WA 98195

<sup>6</sup> Mathematical Sciences Department, Worcester Polytechnic Institute, Worcester, MA 01609 USA

\* Presenting author: Qingyu Wang, Southeast University, Nanjing China, email: 1263800783@qq.com.

†Corresponding author: Dalin Tang, Southeast University, Nanjing China; Mathematical Sciences Department, Worcester Polytechnic Institute, Worcester, MA 01609, email: [dtang@wpi.edu](mailto:dtang@wpi.edu)

## Abstract

Patient-specific vessel material properties are in general lacking in image-based computational models, limiting the accuracy of their stress/strain calculations. A noninvasive approach of combining in vivo 3D multi-contrast and Cine magnetic resonance imaging (MRI) and computational modeling was introduced to quantify patient-specific carotid plaque material properties for potential plaque model improvements. Carotid plaque stress and strain conditions with in vivo and old material model were investigated. A computational plaque stress index (CPVI) was proposed to combine mechanical analysis, plaque morphology and compositions for more complete carotid plaque vulnerability assessment.

In vivo 3D multi-contrast and Cine MRI carotid plaque data were acquired from 8 patients with follow-up (18 months) with written informed consent obtained. 3D thin-layer model and an established iterative procedure were used to determine parameter values in the Mooney-Rivlin models for the 81 slices from 16 plaque samples. Effective Young's Modulus (YM) values were calculated for comparison and analysis.

The average YM, circumferential shrink (C-Shrink) and lumen circumference variation measure by Cine MRI of the 81 slices was 411 kPa, 5.62%, and 8.91%, respectively. Average YM values by vessel varied from 109 kPa (softest) to 922 kPa (stiffest), a 746% difference. The average absolute variation of average stress values from 16 carotid plaques were 16.42% between in vivo material model and old material model, where 8 cases had in vivo material model stress greater than old material model stress and 8 cases had old material model stress greater than in vivo material model stress. The range of absolute variation values was [0.29%, 30.98%]. The average absolute variation of average strain values from 16 carotid plaques were 71.99% between in vivo material model and old material model, where 9 cases had in vivo material model strain greater than old material model strain and 7 cases had old material model strain greater than in vivo material model strain. The range of absolute variation values was [2.82%, 377.34%]. YM values showed positive correlation with Max stress ( $r=0.3531$ ,  $p=0.1797$ ) and critical stress ( $r=0.5733$ ,  $p=0.0202$ ). YM values also showed strong negative correlation with Max strain ( $r=-0.8246$ ,  $p<0.0001$ ) and critical strain ( $r=-0.7376$ ,  $p=0.0011$ ). The five intervals (unit: kPa) [0, 46.8), [46.8,

80), [80, 92), [92, 103), and [103,  $+\infty$ ) from in vivo material models were used for CPVI values of 0, 1, 2, 3 and 4, respectively. The optimized agreement rate was 85.19%.

In vivo carotid vessel material properties have large variations from patient to patient. The use of patient-specific material properties in plaque models could potentially improve the accuracy of model stress/strain calculations. Large-scale studies are needed to further demonstrate that CPVI has the potential to improve the current image-based screening and plaque vulnerability assessment schemes.

**Keyword:** Atherosclerotic plaque; magnetic resonance imaging (MRI); material properties; stress/strain calculation; carotid artery modeling.

## 1. Introduction

Cardiovascular diseases are the major cause of death in the world [1]. Atherosclerotic plaques may rupture without warning and cause fatal clinical events such as heart attack and stroke. Mechanisms for plaque progression and rupture are not well understood. It has been accepted that mechanical forces may play an important role in plaque rupture process and should be considered in an integrated way with plaque morphology and composition for possible improvement of plaque assessment schemes [2]. Currently, screening and diagnosis of patients with atherosclerotic plaques are based on medical images such as magnetic resonance image (MRI), ultrasound, intravascular ultrasound (IVUS), computerized tomography (CT), or optical coherence tomography (OCT). Increasing evidences showed that such medical imaging technologies are not enough to identify those victims before the event occurs [3]-[4]. It has been hypothesized that image-based plaque models and mechanical stress and strain conditions may be useful for more accurate plaque vulnerability assessment and prediction of future clinical events.

In recent years, MRI techniques have shown great potential to non-invasively quantify plaque size, shape and components (fibrous cap, lipid-rich necrotic core and calcification/inflammation) [5]. Yuan et al. developed multi-contrast techniques to improve the quality of MR-images and to better differentiate various components of the plaque [6]-[7]. With the advances of medical imaging technologies [6]-[9], image-based computational models have been introduced to calculate plaque stress/strain conditions and investigate their association with plaque progression and rupture [10]-[21]. However, the accuracy of the computational results is heavily dependent on the data and assumptions used by those models. Data needed for image-based plaque computational models include: a) plaque morphology and components; b) vessel and plaque component material properties; and c) blood flow and pressure conditions [16]. While many image-based models used patient-specific plaque morphology data, patient-specific vessel material properties are lacking in those models [10]-[24]. Non-invasive techniques to obtain in vivo patient-specific vessel material properties are needed to further improve in vivo image-based plaque models [25]-[27].

Considerable efforts have been made by several research groups to quantify mechanical material properties of atherosclerotic vessels. Smoljkić et al. proposed a non-invasive, energy-based assessment of patient-specific material properties of arterial tissue [26]. Their results showed that imposing conditions on strain energy can provide a good estimation of carotid material properties from the non-invasively measured pressure and diameter data. Czernuszewicz et al. performed some preliminary study of non-invasive in vivo characterization of human carotid plaques with acoustic radiation force impulse ultrasound. Their method was able to differentiate soft tissues from

stiffer tissues with histological validations [27]. Liu et al. introduced a non-invasive approach to quantify patient-specific vessel material properties and plaque circumferential shrinkage rate between in vivo and “no-load” vessel geometries [28]. Their material properties and circumferential shrinkage rate were calculated by 2D plaque models. Their results showed that effective Young’s Modulus (YM) from the 12 human carotid arteries varied from 137 kPa to 1435 kPa and vessel circumferential shrinkage to “no-load” condition varied from 6% to 32%. Overall, quantified patient-specific shrinkage rate using in vivo data are rare in the current literature.

The foundation for plaque classifications was established by Stary et al. in a series of American Heart Association (AHA) committee reports on vascular lesions of Council on Arteriosclerosis which provided a histological lesion classification scheme [29]-[31]. Among the AHA Type I – VIII lesions, Type I-IV are considered stable (I-III) or minimally unstable (IV). Types V (lipid-rich), VI (complex), VII (calcified), and VIII (fibrotic) are the advanced plaques capable of rupture. Using non-invasive MRI techniques, Cai et al. developed a classification system for carotid plaques based on in vivo MRI [32]. Tang et al. introduced a “local maximum stress hypothesis” to identify the critical site and stress conditions in the plaque and proposed an ex vivo MRI-based computation plaque vulnerability index (CPVI) to assess plaque vulnerability [14][33]-[34].

In this paper, a non-invasive approach [28] of combining 3D multi-contrast MRI, in vivo Cine MRI and computational 3D thin-layer model [35] was used to quantify patient-specific carotid plaque material properties and circumferential shrinkage rates. A thin-layer modeling method was used to quantify the impact of patient-specific vessel material properties on stress and strain predictions [17]. These methods and results will fill a gap in the current literature. For plaque vulnerability assessment, a stress-based computational plaque vulnerability index (CPVI) was introduced and its value was assigned for all 81 slices using stress values from models with patient-specific material data and old material data. The resulting CPVI classifications were compared with a morphological plaque severity index (MPSI) which was defined based on plaque morphological characteristics known to correlate with plaque vulnerability [32].

## **2. Methods**

### *2.1 MRI Data Acquisition.*

Serial MRI data of carotid atherosclerotic plaques from 8 patients (5 male, 3 female; age: 62–83, mean=71) were acquired at the University of Washington (UW), Seattle by the Vascular Imaging Laboratory (VIL) using protocols approved by the UW Institutional Review Board and with written informed consent obtained. For each patient, MRI slices at baseline (Time 1, T1) and follow-up (Time 2, T2, Scan time intervals were about 18 months) were matched up using vessel bifurcation, stenosis features and with careful review by the MRI group. Cuff systolic and diastolic arm pressure was recorded for modeling use. In vivo Cine and 3D multi-contrast MR images of the carotid arteries were acquired using a 3.0T whole-body scanner (Philips Achieva, R2.6.1, Best, The Netherlands) and a dedicated 8-channel, phased array carotid coil. The carotid bifurcation was located on 2D TOF (Time of Flight) and oblique black blood MR images. A 3.5cm region centered on the carotid bifurcation was imaged by high-resolution axial bright and black blood imaging. Detailed data acquisition and segmentation procedures were published before and are omitted here [11][28]. For each patient, locations with Cine sequence and nearly-circular lumen cross-section were selected for calculating the material parameter values in the modified Mooney-Rivlin model [11][28]. Figure 1 gives 5 selected MRI slices with segmented contour plots of the plaque.

(a) In Vivo MRI Images and segmented contours

(b) 3D Geometry

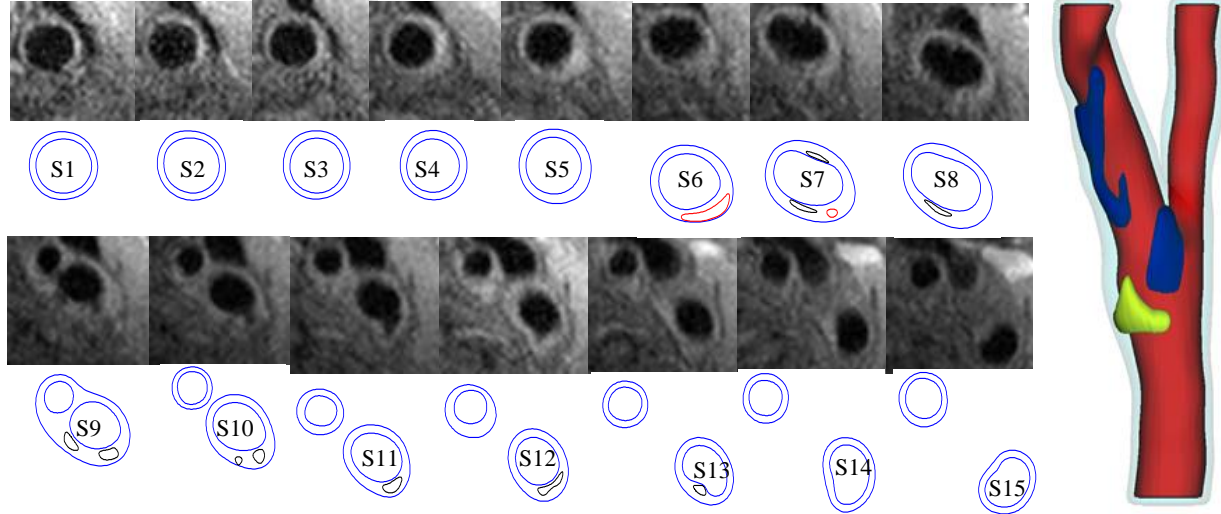


**Figure 1.** A plaque example showing MRI slices, segmented contours, and re-constructed geometry. (a) In vivo MR-images and segmented contour plots showing plaque components (Blue: lumen, vessel wall; black: calcification; red: lipid core); (b): 3D reconstructed geometry (Red: lumen; light blue: vessel; blue: calcification; yellow: lipid core).

## 2.2 Computational Models, Mesh Generation and Solution Methods.

A 3D thin-layer modeling approach introduced by Huang et al. [35] was used to determine material parameter values in our selected material model. For every slice that Cine data was available, a thin slice thickness (0.5 mm) was added to make a 3D thin-layer model (Figure 2). The carotid artery was assumed to be hyperelastic, isotropic, incompressible and homogeneous. The nonlinear modified Mooney-Rivlin (M-R) model was selected to describe the material properties of the vessel wall [36][37]. The strain energy function was given by:

$$W = c_1(I_1 - 3) + c_2(I_2 - 3) + D_1[\exp(D_2(I_1 - 3)) - 1], \quad (1)$$

$$I_1 = \sum C_{ii}, \quad I_2 = \frac{1}{2}[I_1^2 - C_{ij}C_{ij}], \quad (2)$$

where  $C = [C_{ij}] = X^T X$  is the right Cauchy-Green deformation tensor;  $I_1$  and  $I_2$  are the invariants of  $C$ ;  $X = [X_{ij}] = \left[ \frac{\partial x_i}{\partial a_j} \right]$  is the deformation gradient;  $c_1$ ,  $c_2$ ,  $D_1$  and  $D_2$  form the material parameter set. The modified Mooney-Rivlin model was selected because it was able to fit carotid artery vessel properties measured by uniaxial and biaxial mechanical testing data and good agreement was obtained [38]. According to our previous literatures [11][17], material parameters  $c_i$  and  $D_i$  ( $i=1,2$ ) were chosen to match experimental measurements: old vessel material/fibrous cap,  $c_1=36.8$  kPa,  $D_1=14.4$  kPa,  $D_2=2$ ; lipid core/hemorrhage,  $c_1=2$  kPa,  $D_1=2$  kPa,  $D_2=1.5$ ; calcification,  $c_1=368$  kPa,  $D_1=144$  kPa,  $D_2=2.0$ ; loose matrix,  $c_1=18.4$  kPa,  $D_1=7.2$  kPa;  $D_2=1.5$ .  $c_2 = 0$  for all materials [17].

(a) Created Lines connecting data points and dividing lines for a slice.

(b) Add slice thickness to make 3D thin-wall model

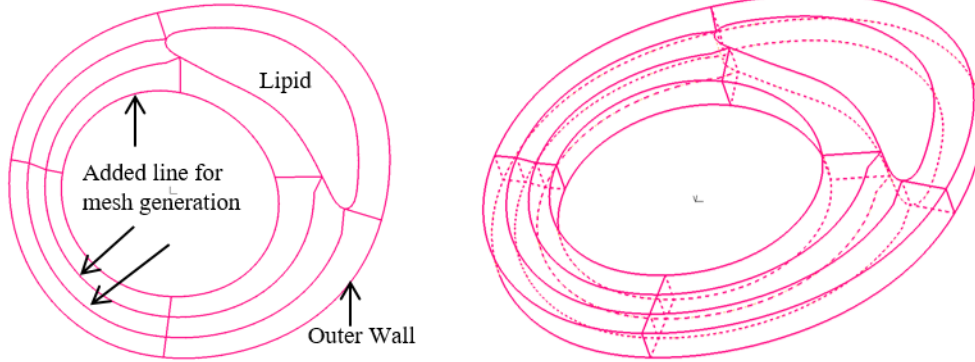


**Figure 2.** Thin-layer model construction.

For each 3D thin-layer model, a 10% axial shrinkage rate was applied. Then an iterative procedure [28] was followed to adjust the parameter values in the modified M-R model and the circumferential shrinkage rate to match both maximum and minimum Cine lumen circumferences corresponding to systolic and diastolic pressures. The details of the iteration procedure were described in our previous paper [28]. The 3D thin-layer model for each iteration was solved by ADINA (ADINA R & D, Watertown, MA). The stress-stretch relationship for the Mooney-Rivlin model is given by:

$$\sigma = \lambda \frac{dW}{d\lambda} = 2\lambda(\lambda - \lambda^{-2}) \left( c_1 + D_1 D_2 e^{D_2 \left( \lambda^2 + \frac{2}{\lambda} - 3 \right)} \right), \quad (3)$$

where  $\sigma$  is Cauchy stress, and  $\lambda$  is stretch ratio. In order to facilitate comparison, it is easier to use a single parameter to compare vessel stiffness from different patients or slices. The effective Young's modulus (YM)  $E$  for the stretch ratio interval [1.0, 1.3] is defined as:

$$\sigma = E(\lambda - 1), \quad (4)$$

The least-squares technique was used to calculate the YM values that best fit the M-R model.

### 2.3 Definition and Calculation of Critical Stress.

It is known that thin plaque cap is closely related to plaque rupture. Thus all locations where a thin region covers a plaque component were considered as candidate critical sites. It should be noted that our “thin region” includes fibrous cap over a lipid core, as well as “cap” over calcification and other plaque components. The site with the maximum Stress (maximum principal stress) value among all the candidate sites was defined as the critical site, and the stress value at this site was defined as the critical stress [33][34]. For slices without any components, critical stress was defined as zero since these slices are very stable.

### 2.4 Assignment of Morphological Plaque Severity Index (MPSI).

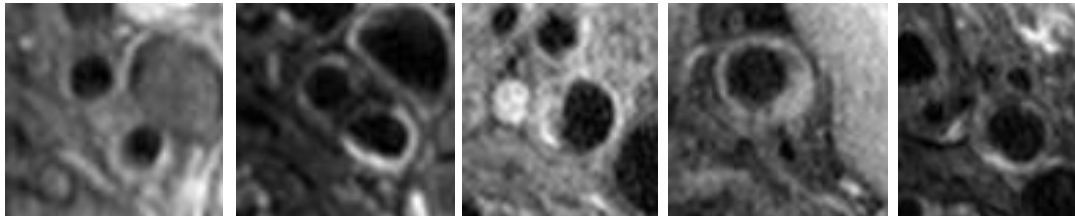
Since histological data is in general not available for in vivo studies, a morphological plaque severity index (MPSI) was introduced (Table 1) and assigned to each segmented MRI slice based on plaque morphological features known to correlate with plaque vulnerability from histopathological studies [39]-[41]. These features include: 1) the size and distribution of the soft lipid rich necrotic core (LRNC); 2) the fibrous cap thickness (which correlates with plaque

stability); and 3) the presence of ulcer, intraplaque hemorrhage and thrombi. MPSI values (0, 1, 2, 3 to 4) indicate the level of increasing severity. The MPSI definitions are closely associated with the AHA (American Heart Association) lesion type classifications (see Table 1). Figure 3 presents 5 representative slices with above described morphological characteristics.

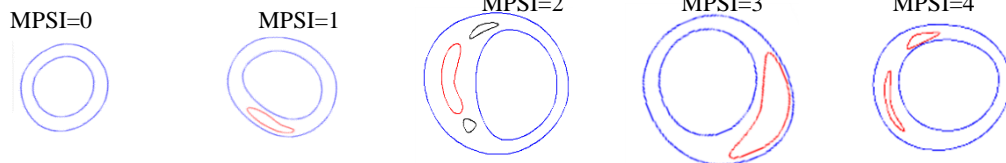
**Table 1.** Morphological plaque vulnerability index (MPSI) classifications and comparison with AHA classifications.

MPSI Category	Corresponding AHA lesion types (modified)	Description	Level of vulnerability
0	I or II	Normal or nearly normal wall.	Very stable
1	III	Moderate intimal thickening, no extracellular lipid, calcification or significant inflammation.	Stable
2	IV/V with less than 30% NC by area; or VII; or VIII	Advanced lesion with small necrotic core (<30% of plaque size), or can be fibrotic or calcified, thick fibrous cap (> 200 $\mu$ m).	Slightly unstable
3	IV/V with 30-40% NC by area	Advanced lesion with Moderate lipid core (30-40% of plaque size) and fibrous cap (150-200 $\mu$ m).	Moderately unstable
4	IV/V with > 40% NC by area; or VI	Advanced lesion with a very large necrotic core (>40%), thin fibrous cap (<150 $\mu$ m), or with fibrous cap rupture, ulceration, or intraplaque hemorrhage.	Very unstable

(a) In Vivo MRI images of selected plaques with different classifications.



(b) Segmented contours



(c) Critical Site and Critical Stress (kPa) on Stress Band Plot

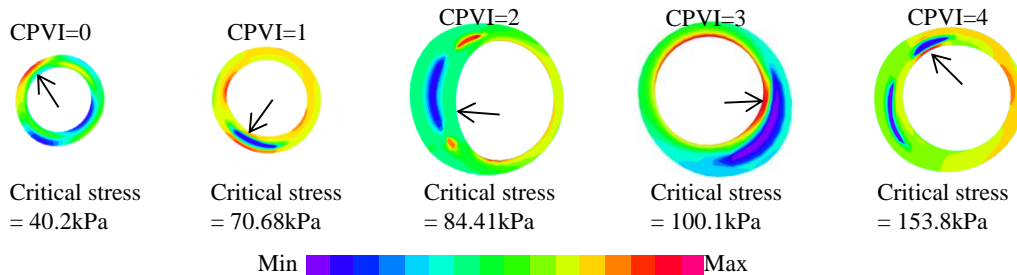


**Figure 3.** Plaque samples showing morphological features and critical stress values for plaque classifications. (a) In vivo MR-images; (b) segmented contour plots showing plaque components (Black: calcification; Red: Lipid core); (c) stress plots showing critical stress of corresponding slices; CPVI values were calculated based on critical stress values at critical sites.

## 2.5 CPVI Assignment and Data Analysis.

Each slice was assigned a CPVI value (0, 1, 2, 3 or 4) according to its critical stress by using five stress intervals, which were determined to have best match rate with MPSI. Correlations between CPVI values and plaque morphological features including lipid core size, cap thickness and normalized wall index were analyzed. Average stress/strain and critical stress/strain on the lumen and all the cap nodes covering the lipid-rich pool were recorded for comparison. To be clear, since stress and strain are tensors, maximum principal stress and maximum principal strain were taken as the scalar representatives of stress and strain to present our results, respectively. Correlation studies were performed using standard student t-test method.

## 3. Results

### 3.1 In vivo patient-specific vessel material properties based on Cine MRI data.

Stress-Stretch Ratio curves from Mooney-Rivlin models for the 16 plaque samples are presented by Figure 4 using average parameter values of slices with Cine data. Average YM values and circumferential shrinkage [28] (C-Shrink) values from 16 plaque samples were given in Table 2. The average YM values for the stiffest plaque sample (P16) was 922 kPa, 746% higher than that for the softest plaque (P13, YM=109 kPa). This showed that plaque material properties have large variations from patient to patient and patient-specific material properties should be used in plaque models. Average C-shrink value from the 16 samples was 6.51%. The softest sample had 21.7% C-shrink value, while the stiffest sample had a negative C-Shrink value (-1.78%). Negative C-Shrink value means the in vivo slice lumen needed to expand slightly to obtain the zero-load geometry of the 3D thin-layer model so that it could regain the in vivo circumference when 10% axial stretch and pressure were applied. Axial stretch makes the vessel to shrink in radial direction.

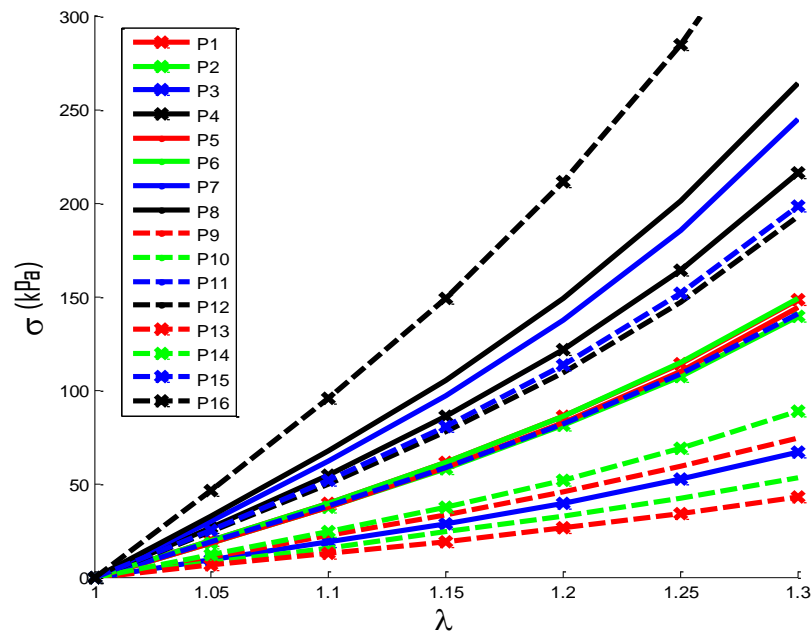


**Figure 4.** Stress-Stretch curves from Mooney-Rivlin Models using parameter values determined from Cine MRI for the 16 plaque samples studied.

**Table 2.** Average material parameter values and circumferential shrinkage for 16 human carotid plaque samples based on Cine MRI data. Due to axial shrink applied to the 3D thin-layer model, some C-Shrink values in 3D thin-layer model were negative.

Plaque	Cir <sub>Max</sub>	Cir <sub>Min</sub>	$\delta_{Cir}$	P	C <sub>1</sub>	D <sub>1</sub>	YM	C-Shrink
	(cm)	(cm)	(%)	(mmHg)	(kPa)	(kPa)	(kPa)	(%)
P1	2.564	2.350	8.35	(120,80)	34.6	14.6	370	7.40
P2	2.328	2.163	7.11	(120,80)	34.8	12.9	348	6.26
P3	2.415	2.119	12.3	(120,70)	19.5	5.31	169	12.3
P4	2.208	2.050	7.15	(141,72)	37.5	25.3	531	1.05
P5	2.089	1.903	8.90	(130,70)	30.0	15.3	357	4.51
P6	2.130	1.950	8.44	(143,80)	34.3	14.7	371	4.11
P7	2.952	2.747	6.93	(146,81)	41.7	28.9	601	2.45
P8	2.073	1.942	6.33	(146,81)	48.3	30.1	650	1.07
P9	2.341	2.094	10.6	(100,60)	28.8	3.66	191	7.48
P10	1.301	1.150	11.6	(100,60)	20.6	2.61	137	9.88
P11	2.136	1.906	10.8	(143,73)	35.0	13.1	352	4.56
P12	2.658	2.389	10.1	(143,73)	38.2	21.1	476	3.96
P13	1.537	1.306	15.0	(143,90)	16.3	2.16	109	21.7
P14	2.018	1.801	10.8	(143,91)	23.3	7.84	222	14.7
P15	2.127	1.933	9.11	(143,65)	41.5	21.0	492	0.92
P16	2.191	2.075	5.28	(143,65)	66.4	43.4	922	-1.78
Ave	2.192	1.992	9.3	(133,74)	34.4	16.4	394	6.51

### 3.2 Impact of patient-specific material properties on stress/strain calculations.

To show impact of patient-specific material properties on stress/strain calculations, we compare models using patient-specific material properties with models using material parameters from the literature (referred to as old material) [17]. Figure 5 gives an example to show the stress/strain differences from the two models. Average lumen stress and strain values for the 16 plaque samples calculated by the 3D thin-layer model using in vivo patient-specific material and old material are given in Table 3. The differences of average stress ( $\Delta_{stress}$ ) and average strain ( $\Delta_{strain}$ ) between in vivo material and old material models are given by:

$$\Delta_{stress} = |\text{stress}_1 - \text{stress}_2| / \text{stress}_2, \quad (5)$$

$$\Delta_{strain} = |\text{strain}_1 - \text{strain}_2| / \text{strain}_2, \quad (6)$$

where  $\text{stress}_1$  and  $\text{strain}_1$  are the average stress and strain values, respectively, calculated using the in vivo material model, and  $\text{stress}_2$  and  $\text{strain}_2$  are the average stress and strain values, respectively, calculated using the old material model. The average absolute variation of average stress values from 16 carotid plaques were 16.42%. The range of  $\Delta_{stress}$  values was [0.29%, 30.98%]. The average absolute variation of average strain values from 16 carotid plaques were 71.99%. The range of  $\Delta_{strain}$  values was [2.82%, 377.34%]. It shows using patient-specific material properties in computational models would lead to significant improvement on accuracy of plaque stress and strain calculation. Strain calculation is more sensitive to material stiffness changes.

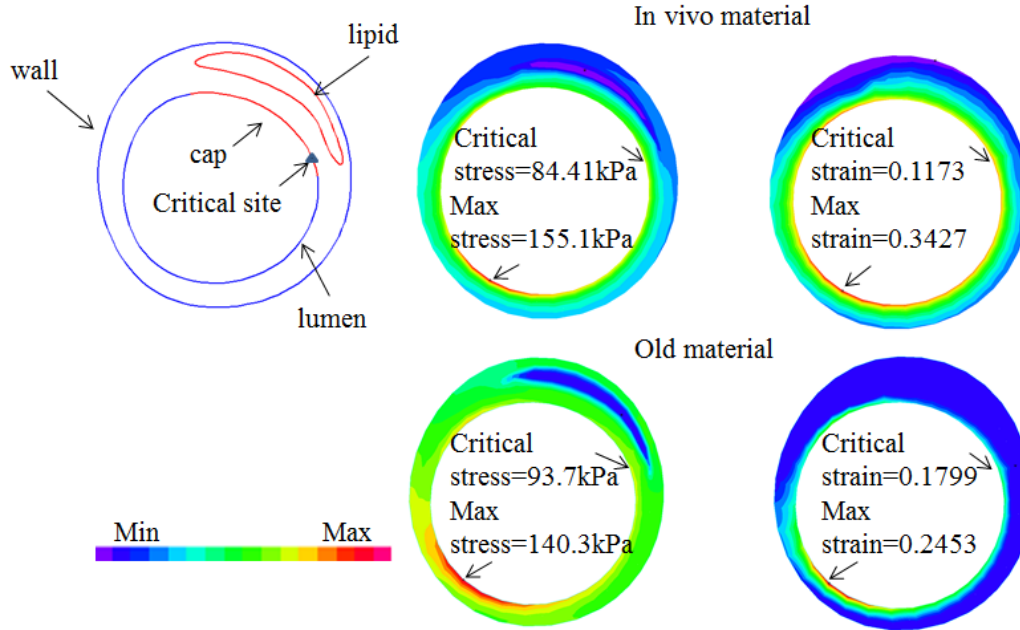


**Figure 5.** Stress and strain differences from models using patient-specific material and old material (in vivo material:  $C_1=20\text{kPa}$ ,  $D_1=1.857\text{kPa}$ ,  $D_2=2$ ; old material:  $c_1=36.8\text{kPa}$ ,  $D_1=14.4\text{kPa}$ ,  $D_2=2$ ; lipid core:  $c_1=2\text{kPa}$ ,  $D_1=2\text{kPa}$ ,  $D_2=1.5$ ;  $c_2 = 0$  for all materials.)

**Table 3.** The average stress and strain values for 16 carotid plaque samples based on MRI data by using in vivo material model and old material [17] model.

Plaque	P (mmHg)	In vivo material		old material		Variation	
		stress	strain	stress	strain	$(\Delta_{\text{stress}})$	$(\Delta_{\text{strain}})$
		(kPa)		(kPa)		(%)	(%)
P1	(120,80)	92.30	0.2745	109.78	0.1952	15.92	40.63
P2	(120,80)	81.75	0.1862	101.34	0.1811	19.33	2.82
P3	(120,70)	78.25	0.3540	69.09	0.1332	13.26	165.77
P4	(141,72)	94.31	0.1345	87.31	0.1657	8.02	18.83
P5	(130,70)	89.82	0.2076	89.56	0.1683	0.29	23.35
P6	(143,80)	81.89	0.1644	93.64	0.1774	12.55	7.33
P7	(146,81)	113.16	0.1295	100.68	0.1865	12.40	30.56
P8	(146,81)	111.71	0.1375	98.27	0.1817	13.68	24.33
P9	(100,60)	55.95	0.2499	76.42	0.1408	26.79	77.49
P10	(100,60)	43.92	0.3107	58.67	0.1196	25.14	159.78
P11	(143,73)	97.00	0.1975	101.86	0.1900	4.77	3.95
P12	(143,73)	124.88	0.1860	133.75	0.2283	6.63	18.53
P13	(143,90)	96.27	0.6721	73.50	0.1408	30.98	377.34
P14	(143,91)	113.94	0.3978	91.32	0.1686	24.77	135.94
P15	(143,65)	92.96	0.1661	117.40	0.2155	20.82	22.92
P16	(143,65)	139.63	0.1173	109.59	0.2030	27.41	42.22
Ave	(133,74)	94.23	0.2429	94.51	0.1747	16.42	71.99
Min	(100,60)	43.92	0.1173	58.67	0.1196	0.29	2.82
Max	(146,81)	139.63	0.6721	133.75	0.2283	30.98	377.34

### 3.3 Critical stress and strain using patient-specific vessel material data.

The average maximum and critical stress and strain values from 16 plaque samples were given in Table 4. For 16 carotid plaques, systolic blood pressure shows positive correlation with maximum (Max) stress ( $r=0.5589$ ,  $p=0.0244$ ) and critical stress ( $r=0.6168$ ,  $p=0.0109$ ). It indicates that systolic blood pressure has significant impact on stress calculations. YM values showed positive correlation with critical stress ( $r=0.5733$ ,  $p=0.0202$ ), but its correlation with maximum stress was not significant ( $r=0.3531$ ,  $p=0.1797$ ). The YM value shows strong negative correlation with maximum strain ( $r=-0.8246$ ,  $p<0.0001$ ) and critical strain ( $r=-0.7376$ ,  $p=0.0011$ ).

**Table 4.** Summary of stress and strain values and other risk factors for 16 human carotid plaque samples from 3D thin-layer model with patient-specific vessel material data.

Plaque	PB	WT	P	YM	Stress (kPa)		Strain	
	(%)	(mm)	(mmHg)	(kPa)	Max	Critical	Max	Critical
P1	32	0.911	(120,80)	370	105.22	72.51	0.2904	0.1865
P2	34.2	0.883	(120,80)	348	105.41	62.6	0.2575	0.1425
P3	49.4	1.337	(120,70)	169	153.16	78.09	0.5491	0.3698
P4	46.5	1.145	(141,72)	531	127.07	84.21	0.2003	0.1385
P5	47.3	1.126	(130,70)	357	131.23	86.97	0.3001	0.2268
P6	42.1	1.059	(143,80)	371	113.49	67.91	0.2239	0.1325
P7	43.9	1.364	(146,81)	601	159.08	114.73	0.1619	0.1331
P8	49.8	1.327	(146,81)	650	144.46	116.33	0.1607	0.1256
P9	39.4	1.077	(100,60)	191	103.09	61.64	0.4479	0.2794
P10	64.1	1.293	(100,60)	137	67.88	57.89	0.4507	0.407
P11	39	0.872	(143,73)	352	111.25	82.05	0.2352	0.1641
P12	38	1.016	(143,73)	476	227.93	168.45	0.3046	0.2292
P13	49.7	0.98	(143,90)	109	127.26	87.59	0.7809	0.6467
P14	44.3	1.159	(143,91)	222	160.53	111.51	0.4899	0.3794
P15	40.2	1.098	(143,65)	492	114.23	82.47	0.2037	0.1465
P16	38.4	0.873	(143,65)	922	149.73	132.05	0.1173	0.1173
Ave	43.6	1.095	(133,74)	411	131.31	91.69	0.3234	0.2391
Min	32	0.872	(100,60)	109	67.88	57.89	0.1173	0.1173
Max	64.1	1.364	(146,81)	922	227.93	168.45	0.7809	0.6467

### 3.4 CPVI using in vivo material and old material and agreement with MPSI.

Figure 3 (b) and (c) give an example for the MPSI and CPVI groups, respectively. Figure 6 shows that critical stress values correlate much better with MPSI than the maximum (Max) stress values. Figure 6 also shows that critical stress values from in vivo material models correlate much better with MPSI than that from the old material model. A simple numerical code was used to determine five equal stress intervals  $[0, a)$ ,  $[a, 2a)$ ,  $[2a, 3a)$ ,  $[3a, 4a)$ , and  $[4a, +\infty)$  corresponding to CPVI values 0-4 to reach the best agreement between CPVI and MPSI. The five intervals (unit: kPa)  $[0, 46.8)$ ,  $[46.8, 80)$ ,  $[80, 92)$ ,  $[92, 103)$ , and  $[103, +\infty)$  from in vivo material models were used for

CPVI values of 0, 1, 2, 3 and 4, respectively. And the five intervals (unit: kPa) [0, 50.4), [50.4, 82), [82, 91), [91, 140), and [140, +∞) from old material models were used for CPVI values of 0, 1, 2, 3 and 4, respectively. The optimized agreement rate was 85.19% and 83.95%, respectively. The Pearson correlation coefficient between CPVI and MPSI was 0.9103 ( $p < 0.0001$ ) and 0.8661 ( $p < 0.0001$ ), respectively. Table 5 lists number of cases and agreement rate for each MPSI grade group. The ones with MPSI being 3 have the lowest match rates, which are 57.14% and 42.86%, respectively. From the agreement rates, the in vivo results more than 50%. According to the CPVI stress intervals, a plaque will be considered unstable (risk) if its critical stress is higher than 100 kPa from in vivo material models. And a plaque will be considered highly vulnerable (high risk) if its critical stress is higher than 140 kPa.

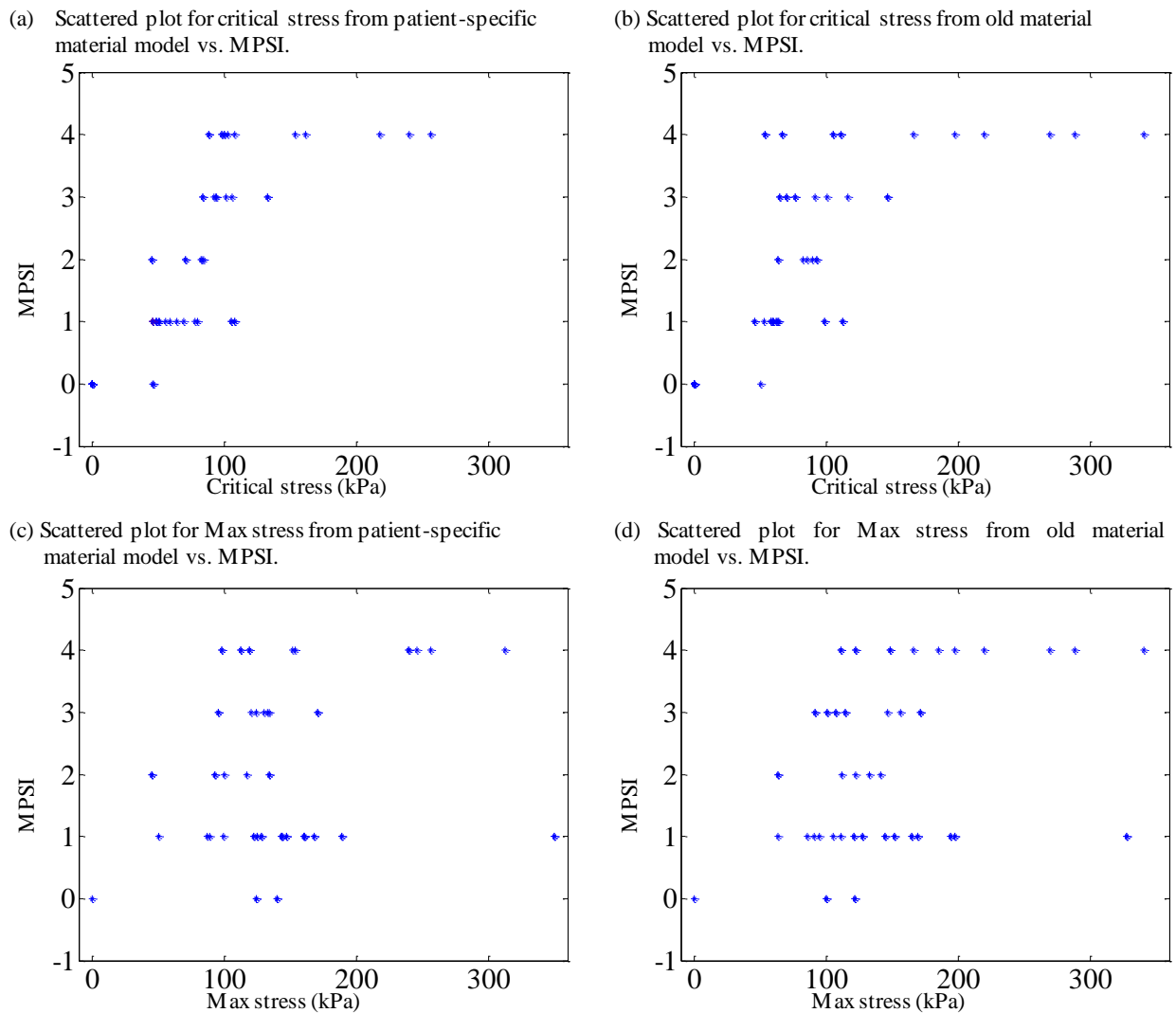


**Figure 6.** Critical stress shows much better correlation with MPSI from 16 carotid plaque samples. (a) Scattered plot for critical stress from patient-specific material model vs. MPSI; (b) Scattered plot for critical stress from old material model vs. MPSI; (c) Scattered plot for Max stress from patient-specific material model vs. MPSI; (d) Scattered plot for Max stress from old material model vs. MPSI.

**Table 5.** Case distributions according to MPSI and agreement rate between CPVI and MPSI

MPSI	Number of slices	Percentage (%)	Agreement Rate (%)	
			in vivo	old
0	44	54.32	100.00	100.00
1	15	18.52	73.33	80.00
2	5	6.17	60.00	60.00
3	7	8.64	57.14	42.86
4	10	12.35	70.00	60.00
All	81	100	85.19	83.95

## 4. Discussion

### 4.1. Significance of in vivo patient-specific vessel material properties.

Most of the research on determining arterial wall material properties has been performed using ex vivo specimens and in vitro experimental techniques. In vivo estimation of patient-specific material properties is scarce, which is a serious limitation for patient-specific plaque models. A noninvasive approach of combining in vivo Cine and 3D MRI and simple 3D thin-layer modeling was introduced to quantify patient-specific vessel material properties and improve model prediction accuracies. Our results from 16 plaques showed that slice YM values could vary from 109 kPa to 922 kPa, 7 times of the lowest YM value. Future studies should render plaque models using patient-specific material properties to quantify their impact on stress/strain calculations.

### 4.2 Vessel material has greater impact on strain predictions.

Using the in vivo material models, the average strain values from 16 plaque samples were 71.99% higher than that from the old material model, while average strain values were only 16.42% higher. Considering that most research reports have been focused on critical stress conditions, our results indicated that plaque mechanical investigations should include both critical stress and strain conditions when the accurate in vivo vessel material properties become available.

### 4.3 Threshold Critical Stress Value for Highly Vulnerable Plaques.

It should be noted that our threshold critical stress value from in vivo material model (103 kPa for CPVI=4) are lower than the threshold value from old material model (140 kPa for CPVI=4) for several reasons: a) Our models were based on in vivo material models could led to different stress predictions; b) Our 81 slices from 16 plaque samples included cases from stable to unstable and the number of CPVI=4 were only 7 slices.

### 4.4 Purpose of Introducing CPVI and Modeling Considerations.

The purpose of introducing CPVI is to have a more complete plaque assessment scheme which includes mechanical factors, plaque morphological features and tissue compositions for possible patient-screening applications. Results from 81 slices suggested that CPVI and MPSI had good agreement on plaque classifications. At the same time, the disagreement cases suggested that CPVI scheme may complement image-only assessment schemes and lead to potential improvements. The present study is the first in vivo case studies quantifying differences between mechanics-image combined and morphology-only assessment schemes.

It should be understood that plaque rupture is a multi-faceted process. CPVI covers only mechanical and morphological factors. We hope CPVI could provide complementing information for plaque assessment that image alone could not provide. Multiple biomarkers from different channels such as cell activities, lumen surface conditions, inflammation, blood conditions (cholesterol level and diabetes, for example) should be jointly considered for more complete and accurate vulnerability assessment.

#### *4.5 Model limitations.*

Cine MRI was used to determine vessel material parameter values, matching in vivo plaque geometries under both systolic and diastolic pressure conditions. Cine MRI is widely accepted to acquire time-dependent vessel motion and deformation. Multi-layer structure and anisotropic material properties of arteries were not considered since MRI does not provide layer information. Cine data provided only circumference variations under cardiac pressure. Another limitation was that location-specific pressure measurement was not available. Currently, arm cuff pressure values are used in most image-based studies. Noninvasive acquisition of intraplaque pressure data remains a challenge.

In computational models, contours for plaque components are generated based on segmentation data, the limitation of MRI resolution have impact on our calculated results. Furthermore, larger patient size will potentially lead to better plaque vulnerability prediction result.

## **5. Conclusion**

Our preliminary results indicated that in vivo carotid vessel material properties have large variations from patient to patient, and vessel stiffness have impact on stress and strain calculations. In vivo material plaque model show significant difference with old material plaque model on stress and strain calculations. These differences showed that using in vivo material model to replace old material model would improve the accuracy of stress and strain calculation.

### **Funding:**

This research was supported in part by NSF grant DMS-0540684 and NIH grant R01 EB004759. Tang's research was also supported in part by National Sciences Foundation of China grant 11672001 and a Jiangsu Province Science and Technology Agency grant BE2016785.

### **Conflict of Interest:**

The authors declare that they have no conflict of interest.

### **Ethical approval:**

This study was approved by the University of Washington Institutional Review Board and with written informed consent obtained. All procedures performed in studies involving human participants were in accordance with the ethical standards of the institutional and/or national research committee and with the 1964 Helsinki declaration and its later amendments or comparable ethical standards.

## Reference

1. World Health Organization. Global Atlas on cardiovascular disease prevention and control. Geneva: World Health Organization; 2011.
2. Fuster, V. The Vulnerable Atherosclerotic Plaque: Understanding, Identification, and Modification, Edited by V. Fuster, J. F. Cornhill, R. E. Dinsmore, J. T. Fallon, W. Insull, P. Libby, S. Nissen, M. E. Rosenfeld, and W. D. Wagner. AHA Monograph Series. Armonk, NY: Futura Publishing, 1998.
3. Naghavi, M., P. Libby, E. Falk, S. W. Casscells, S. Litovsky, J. Rumberger, J. J. Badimon, C. Stefanadis, P. Moreno, G. Pasterkamp, Z. Fayad, P. H. Stone, S. Waxman, P. Raggi, M. Madjid, A. Zarrabi, A. Burke, C. Yuan, P. J. Fitzgerald, D. S. Siscovick, C. L. de Korte, M. Aikawa, K. E. Juhani Airaksinen, G. Assmann, C. R. Becker, J. H. Chesebro, A. Farb, Z. S. Galis, C. Jackson, I. K. Jang, W. Koenig, R. A. Lodder, K. March, J. Demirovic, M. Navab, S. G. Priori, M. D. Reikter, R. Bahr, S. M. Grundy, R. Mehran, A. Colombo, E. Boerwinkle, C. Ballantyne, W. Jr. Insull, R. S. Schwartz, R. Vogel, P. W. Serruys, G. K. Hansson, D. P. Faxon, S. Kaul, H. Drexler, P. Greenland, J. E. Muller, R. Virmani, P. M. Ridker, D. P. Zipes, P. K. Shah, J. T. Willerson. From vulnerable plaque to vulnerable patient: a call for new definitions and risk assessment strategies: Part I. *Circulation*. 108(14):1664-72, 2003.
4. Naghavi, M., P. Libby, E. Falk, S. W. Casscells, S. Litovsky, J. Rumberger, J. J. Badimon, C. Stefanadis, P. Moreno, G. Pasterkamp, Z. Fayad, P. H. Stone, S. Waxman, P. Raggi, M. Madjid, A. Zarrabi, A. Burke, C. Yuan, P. J. Fitzgerald, D. S. Siscovick, C. L. de Korte, M. Aikawa, K. E. Juhani Airaksinen, G. Assmann, C. R. Becker, J. H. Chesebro, A. Farb, Z. S. Galis, C. Jackson, I. K. Jang, W. Koenig, R. A. Lodder, K. March, J. Demirovic, M. Navab, S. G. Priori, M. D. Reikter, R. Bahr, S. M. Grundy, R. Mehran, A. Colombo, E. Boerwinkle, C. Ballantyne, W. Jr. Insull, R. S. Schwartz, R. Vogel, P. W. Serruys, G. K. Hansson, D. P. Faxon, S. Kaul, H. Drexler, P. Greenland, J. E. Muller, R. Virmani, P. M. Ridker, D. P. Zipes, P. K. Shah, J. T. Willerson. From vulnerable plaque to vulnerable patient: a call for new definitions and risk assessment strategies: Part II. *Circulation*. 108(15):1772-8, 2003.
5. Saam, T, M. S. Ferguson, V. L. Yarnykh, N. Takaya, D. Xu, N. L. Polissar, T. S. Hatsukami, C. Yuan. Quantitative evaluation of carotid plaque composition by in vivo MRI. *Arterioscler Thromb. Vasc. Biol*. 25(1):234-9, 2005.
6. Yuan, C., L. M. Mitsumori, K. W. Beach, K. R. Maravilla. Special review: Carotid atherosclerotic plaque: Noninvasive MR characterization and identification of vulnerable lesions. *Radiology*. 221:285-99, 2001.
7. Yuan, C., L. M. Mitsumori, M. S. Ferguson, N. L. Polissar, D. E. Echelard, G. Ortiz, R. Small, J. W. Davies, W. S. Kerwin, T. S. Hatsukami. In vivo accuracy of multispectral MR imaging for identifying lipid-rich necrotic cores and intraplaque hemorrhage in advanced human carotid plaques. *Circulation*. 104:2051-2056, 2001.
8. Underhill HR, Hatsukami TS, Fayad ZA, Fuster V, Yuan C. MRI of carotid atherosclerosis: Clinical implications and future directions. *Nat Rev Cardiol*.2010; 7(3):165-73.
9. Yuan C, Zhang SX, Polissar NL, Echelard D, Ortiz G, Davis JW, Ellington E, Ferguson MS, Hatsukami TS. Identification of fibrous cap rupture with MRI is highly associated with recent transient ischemic attack or stroke. *Circulation*.2002; 105:181-5.
10. Friedman MH, Krams R, Chandran KB. Flow interactions with cells and tissues: Cardiovascular flows and fluid-structure interactions. *Ann Biomed Eng*. 2010; 38(3):1178-87.
11. Tang D, Teng Z, Canton G, Yang C, Ferguson M, Huang X, Zheng J, Woodard PK, Yuan C. Sites of rupture in human atherosclerotic carotid plaques are associated with high structural stresses: an in vivo MRI-based 3D fluid-structure interaction study. *Stroke*.2009; 40:3258-3263. Featured article on MDlinx.com.
12. Holzapfel GA, Stadler M, Schulze-Bause CA. A layer-specific three dimensional model for the simulation of balloon angioplasty using magnetic resonance imaging and mechanical testing. *Ann Biomed Eng*. 2002; 30(6):753-767.
13. Bluestein D, Alemu Y, Avrahami I, Gharib M, Dumont K, Ricotta JJ, Einav S. Influence of microcalcifications on vulnerable plaque mechanics using FSI modeling. *J Biomech*.2008; 41(5):1111-1118.
14. Teng Z, Canton G, Yuan C, Ferguson M, Yang C, Huang X, Zheng J, Woodard PK, Tang D. 3D critical plaque wall stress is a better predictor of carotid plaque rupture sites than flow shear stress: an in vivo MRI-based 3D FSI study. *J Biomech Eng*.2010; 132(3):031007.
15. Kaazempur-Mofrad MR, Isasi AG, Younis HF, Chan RC, Hinton DP, Sukhova G, Lamuraglia GM, Lee RT, Kamm RD. Characterization of the atherosclerotic carotid bifurcation using MRI, finite element modeling, and histology. *Ann Biomed Eng*. 2004; 32(7):932-946.
16. Tang D, Kamm RD, Yang C, Zheng J, Canton G, Bach RG, Huang XY, Hatsukami TS, Zhu J, Ma G, Maehara A, Mintz GS, Yuan C. Image-based modeling for better understanding and assessment of atherosclerotic plaque

- progression and vulnerability: Data, modeling, validation, uncertainty and predictions. *Journal of Biomechanics*. 2014; 47(4):834–846.
17. Tang D, Yang C, Zheng J, Woodard PK, Sicard GA, Saffitz JE, and Yuan C. 3D MRI-based multi-component FSI models for atherosclerotic plaques: a 3-D FSI model. *Ann. Biomed. Eng.*2004; 32(7): 947-960.
  18. Li ZY, Howarth S, Trivedi RA, U-King-Im JM, Graves MJ, Brown A, Wang LQ, Gillard JH. Stress analysis of carotid plaque rupture based on in vivo high resolution MRI. *J Biomech.*2006; 39(14):2611-2622.
  19. Gao H, Long Q, Das SK, Sadat U, Graves M, Gillard JH, Li ZY. Stress analysis of carotid atheroma in transient ischemic attack patients: evidence for extreme stress-induced plaque rupture. *Ann Biomed Eng.* 2011 Aug;39(8):2203-12.
  20. Gao H, Long Q, Kumar Das S, Halls J, Graves M, Gillard JH, Li ZY. Study of carotid arterial plaque stress for symptomatic and asymptomatic patients. *J Biomech.* 2011 Sep 23;44(14):2551-7. doi: 10.1016/j.jbiomech.2011.07.012. Epub 2011 Aug 6.
  21. Gallo D, Steinman DA, Morbiducci U. An insight into the mechanistic role of the common carotid artery on the hemodynamics at the carotid bifurcation. *Ann Biomed Eng.* 2015 Jan;43(1):68-81. doi: 10.1007/s10439-014-1119-0. Epub 2014 Sep 19.
  22. Yang C, Tang D, Atluri S. Three-dimensional carotid plaque progression simulation using meshless generalized finite difference method based on multi-year MRI patient-tracking data. *Computer Modeling in Engineering and Sciences.*2010; 57(1):51-76.
  23. Yang C, Tang D, Yuan C, Kerwin W, Liu F, Canton G, Hatsukami TS, Atluri S. Meshless generalized finite difference method and human carotid atherosclerotic plaque progression simulation using multi-year MRI patient-tracking data. *Computer Modeling in Engineering and Sciences.*2008; 28(2):95-107.
  24. Yang C, Canton G, Yuan C, Ferguson M, Hatsukami TS, Tang D. Advanced human carotid plaque progression correlates positively with flow shear stress using follow-up scan data: an in vivo MRI multi-patient 3D FSI study. *J Biomech.* 2010; 43(13):2530-8.
  25. Nieuwstadt HA, Fekkes S, Hansen HH, de Korte CL, van der Lugt A, Wentzel JJ, van der Steen AF, Gijsen FJ. Carotid plaque elasticity estimation using ultrasound elastography, MRI, and inverse FEA - A numerical feasibility study. *Med Eng Phys.* 2015 Aug;37(8):801-7.
  26. Smoljkić M, Vander Sloten J, Segers P, Famaey N. Non-invasive, energy-based assessment of patient-specific material properties of arterial tissue. *Biomech Model Mechanobiol.* 2015 Oct;14(5):1045-56.
  27. Czernuszewicz TJ, Homeister JW, Caughey MC, Farber MA, Fulton JJ, Ford PF, Marston WA, Vallabhaneni R, Nichols TC, Gallippi CM. Non-invasive in vivo characterization of human carotid plaques with acoustic radiation force impulse ultrasound: comparison with histology after endarterectomy. *Ultrasound Med Biol.* 2015 Mar;41(3):685-97.
  28. Liu H, Canton G, Yuan C, Yang C, Billiar K, Teng Z, Hoffman AH, Tang D. Using in vivo cine and 3D multi-contrast MRI to determine human atherosclerotic carotid artery material properties and circumferential shrinkage rate and their impact on stress/strain predictions. *J Biomech Eng.* 2012; 134(1):223-233.
  29. Stary, H. C., D. H. Blankenhorn, A. B. Chandler, S. Glagov, Jr. W. Insull, M. Richardson, M. E. Rosenfeld, S. A. Schaffer, C. J. Schwartz, W. D. Wagner, R. W. Wissler. A definition of the intima of human arteries and of its atherosclerosis-prone regions. A report from the Committee on Vascular Lesions of the Council on Arteriosclerosis, AHA. *Circulation.* 85: 391–405, 1992.
  30. Stary, H. C., A. B. Chandler, S. Glagov, J. R. Guyton, Jr. W. Insull, M. Richardson, M. E. Rosenfeld, S. A. Schaffer, C. J. Schwartz, W. D. Wagner, R. W. Wissler. A definition of initial, fatty streak and intermediate lesions of atherosclerosis. A report from the Committee on Vascular Lesions of the Council on Arteriosclerosis, AHA. *Circulation.* 89: 2462–2478, 1994.
  31. Stary, H. C., A. B. Chandler, M. D. Dinsmore, V. Fuster, S. Glagov, Jr. W. Insull, M. E. Rosenfeld, C. J. Schwartz, W. D. Wagner, R. W. Wissler. Definitions of advanced types of atherosclerotic lesions and the histological classification of atherosclerosis. A report from the Committee on Vascular Lesions of the Council on Arteriosclerosis, AHA. *Circulation.* 92:1355–1374, 1995.
  32. Cai, J. M., T. S. Hatsukami, M. S. Ferguson, R. Small, N. L. Polissar, C. Yuan. Classification of human carotid atherosclerotic lesions with in vivo multicontrast magnetic resonance imaging. *Circulation.* 106:1368–1373, 2002.
  33. Tang, D., C. Yang, J. Zheng, P. K. Woodard, J. E. Saffitz, J. D. Petrucci, G. A. Sicard, C. Yuan. Local maximal stress hypothesis and computational plaque vulnerability index for atherosclerotic plaque assessment. *Annals of Biomed Engineering.* 33(12):1789-1801, 2005.
  34. D Tang,Z Teng,G Canton,TS Hatsukami,L Dong, XY Huang, C. Yuan. Local critical stress correlates better than global maximum stress with plaque morphological features linked to atherosclerotic plaque vulnerability: an in vivo multi-patient study. *BioMedical Engineering OnLine.* 8(1):15, 2009

35. Huang X, Yang C, Zheng J, Bach R, Muccigrosso D, Woodard PK, Tang D. 3D MRI-based multicomponent thin layer structure only plaque models for atherosclerotic plaques. *J Biomechanics*.2016; accepted.
36. Bathe KJ, 1996. *Finite Element Procedures*, Prentice Hall, Inc. New Jersey.
37. Bathe KJ, Editor. 2002. *Theory and Modeling Guide, Vol I & II: ADINA and ADINA-F, ADINA R & D, Inc.*, Watertown, MA.
38. Kural MH, Cai M, Tang D, Gwyther T, Zheng J, Billiar KL. Planar biaxial characterization of diseased human coronary and carotid arteries for computational modeling. *J Biomech*. 2012; 45(5):790-798.
39. Cheng, G. C., H. M. Loree, R. D. Kamm, M. C. Fishbein, R. T. Lee. Distribution of circumferential stress in ruptured and stable atherosclerotic lesions, a structural analysis with histopathological correlation. *Circulation*. 87:1179–1187, 1993.
40. Kerwin, W., D. Xu, F. Liu, T. Saam, H. Underhill, N. Takaya, B. Chu, T. Hatsukami, C. Yuan. Magnetic resonance imaging of carotid atherosclerosis: Plaque analysis. *Topics in Magnetic Resonance Imaging*. 18: 371-378, 2007.
41. Long, Q., X. Y. Xu, B. Ariff, S. A. Thom, A. D. Hughes, A. V. Stanton, Reconstruction of blood flow patterns in a human carotid bifurcation: A combined CFD and MRI study, *Journal of Magnetic Resonance Imaging*. 11:299-311, 2000.